Letter

# Quantifying measurement-induced quantum-to-classical crossover using an open-system entanglement measure

Christian Carisch,[1] Alessandro Romito,[2] and Oded Zilberberg[3]
[1]*Institute for Theoretical Physics, ETH Zürich, CH-8093 Zürich, Switzerland*
[2]*Department of Physics, Lancaster University, Lancaster LA1 4YB, United Kingdom*
[3]*Department of Physics, University of Konstanz, 78464 Konstanz, Germany*

(Received 6 April 2023; accepted 11 October 2023; published 29 November 2023)

The evolution of a quantum system subject to measurements can be described by stochastic quantum trajectories of pure states. Instead, the ensemble average over trajectories is a mixed state evolving via a master equation. Both descriptions lead to the same expectation values for linear observables. Recently, there is growing interest in the average entanglement appearing during quantum trajectories. The entanglement is a nonlinear observable that is sensitive to so-called measurement-induced phase transitions, namely transitions from a system-size dependent phase to a quantum Zeno phase with area-law entanglement. Intriguingly, the mixed steady-state description of these systems is insensitive to this phase transition. Together with the difficulty of quantifying the mixed state entanglement, this favors quantum trajectories for the description of the quantum measurement process. Here, we study the entanglement of a single particle under continuous measurements (using the newly developed configuration coherence) in both the mixed state and the quantum trajectories descriptions. In both descriptions, we find that the entanglement at intermediate time scales shows the same qualitative behavior as a function of the measurement strength. The entanglement engenders a notion of coherence length, whose dependence on the measurement strength is explained by a cascade of underdamped-to-overdamped transitions. This demonstrates that measurement-induced entanglement dynamics can be captured by mixed states.

DOI: 10.1103/PhysRevResearch.5.L042031

A quantum system is described by a wave function and, unlike its classical counterpart, can assume several states at once (superposition), where each state is associated with a certain (probability) amplitude. The time evolution of these amplitudes is governed by the famous Schrödinger wave equation [1]. However, when we measure the particle in a specific classical state, the wave function's superposition must abruptly collapse with a state-dependent probability [2–4]. This stochastic process is incompatible with the deterministic Schrödinger equation. Over the years, various attempts have been made to integrate the measurement postulate into the framework of continuous wave function evolution by coupling the system to a detector [3–7]. In this case too, however, the quantum system effectively becomes open in the presence of the out-of-equilibrium detectors, and measurement backaction on the system requires a statistical average over the quantum detector states. As a result, the wave function's time evolution under a sequence of measurements can be described by a quantum trajectory [4,8]: the continuous evolution governed by the Schrödinger equation is interrupted by stochastic jumps whenever a measurement occurs.

Due to this emergent stochasticity, we can also consider the evolution of the average probability density distribution of the measurement outcomes. This engenders a continuous evolution of the system's density matrix using Lindblad's master equation [9,10]. Alternatively, the Lindblad master equation can be derived from the Schrödinger equation of the combined system and detector by tracing out the detector's degree of freedom in the limit of weak system-detector coupling and Markovian detector's dynamics [4,5,8,11,12]. Note that different assumptions on the detector and its coupling to the system lead to different types of master equations, including Nakajima-Zwanzig [13,14], Bloch-Redfield [15–17], or the time-convolutionless master equations [18–21], can incorporate higher orders of system-detector coupling [22–24], and lead to exotic measurement protocols [25–28]. For the purpose of this work, we will remain within the Lindblad master equation framework.

Recently, the equivalence between the quantum trajectory and Lindblad master equation descriptions has been challenged in the context of measurement-induced phase transitions. Here, the competition between the coherent evolution and the measurement collapse leads to a phase transition that is commonly quantified using an entanglement measure as an order parameter. Specifically, one observes a transition from a critical phase with system-size dependent entanglement for weak measurements to an area-law quantum Zeno phase for strong measurements [30–34], which has been reported in early experiments [35,36].

Crucially, the order parameters used to quantify measurement-induced phase transitions are nonlinear functions of the density matrix, leading to a different outcome

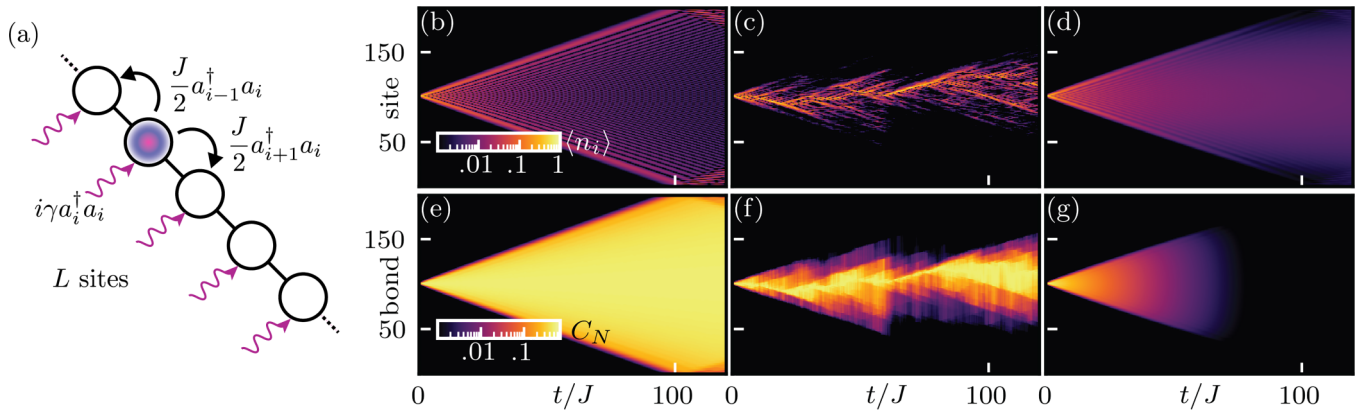


FIG. 1. (a) Setup: spinless particles hopping with amplitude $J/2$ on a chain of length $L$ [cf. Eq. (1)]. The particles are monitored with strength $\gamma$ [cf. Eqs. (2) and (3)]. (b)–(d) Evolution of local densities $\langle n_i \rangle$. (e)–(g) Evolution of the configuration coherence $C_N$. (b) and (e): Without monitoring ($\gamma = 0$), the evolution is ballistic and supported by extensive entanglement. (c) and (f): Quantum random walk of a single quantum trajectory for measurement strength $\gamma = 0.1$ [cf. Eq. (2)]. The ballistic evolution becomes interrupted by stochastic collapses. (d) and (g): Quantum-to-classical crossover of the mixed state evolution for measurement strength $\gamma = 0.04$ (cf. Eq. (3); throughout this work using QuTiP [29]). The evolution changes from ballistic at short times to diffusive at long times.

when averaging over sample paths or over the (density matrix) ensemble. Curiously, the mixed state described by the Lindblad master equation shows no such phase transition because at long times, the disentangling measurements will always defeat the entangling effects [30,32,37,38]. Moreover, while the entanglement of quantum trajectories can be efficiently measured by means of the entanglement entropy [39], it is still notoriously difficult to extract the entanglement of the mixed state [40,41]. This striking difference has sparked a discussion about which of the quantum measurement descriptions is more revealing, with significant implications for a wide range of research fields, including quantum devices in the NISQ era [42,43] and quantum metrology [44–46].

Here, we resolve the discrepancy between the two descriptions in capturing the measurement-induced entanglement dynamics. To quantify entanglement in both the Lindblad and the quantum trajectory descriptions, we employ the recently developed configuration coherence [47,48]. For simplicity, we study a single particle in the presence of local density measurements. The corresponding dynamics of monitored free fermions has been studied at trajectory levels [49–60] showing the presence of a measurement-induced area-law phase. In the Lindblad description the detector resembles a dephasing environment. As the density matrix thermalizes in the long-time limit, we study instead the short- and intermediate-time behavior of the system. Here, we find that the quantum trajectories and the mixed state show a qualitatively similar entanglement evolution, and are able to extract a notion of coherence length using both approaches. We further show that this coherence length saturates for large values of the measurement strength. The saturation of the coherence length can be understood as a cascade of underdamped-to-overdamped transitions in the Liouvillian eigenmodes [61]. Our results enable the investigation of the measurement-induced entanglement phase transition in the context of mixed states.

We consider a spinless particle hopping on a 1D chain in the presence of local density measurements, see Fig. 1(a). The particle's free evolution is described by the Hamiltonian

$$H = \frac{J}{2}\sum_{i=1}^{L-1}[a_i^\dagger a_{i+1} + a_{i+1}^\dagger a_i], \tag{1}$$

with $J$ the hopping amplitude, $a_i^\dagger$ ($a_i$) the creation (annihilation) operator, and $L$ the chain's length. For convenience, we set $J = 1$. The spectrum $\epsilon(k)$ of the closed system (1) is associated with standing waves $|\tilde{k}_m\rangle$ with group velocities $v_m \equiv (\partial\epsilon/\partial k)_{k=\tilde{k}_m} = \sin(\pi m/(L+1))$, $m = 1, \ldots, L$. In the following, we inject the particle into the center of the chain, $|\psi(t=0)\rangle = |L/2\rangle := a_{L/2}^\dagger|0\rangle$, where $|0\rangle$ is the vacuum state. Such a localized particle overlaps with all the eigenmodes simultaneously, resulting in a ballistic quantum random walk [62]. Its characteristic density envelope evolves linearly with velocity $v_{L/2} \approx 1$ of the fastest eigenmode [63], see Fig. 1(b).

In general, measurements of the particle will modify the coherent ballistic evolution [64–67]. As a simple model of quantum measurement, we consider that the chain's sites are capacitively coupled to independent detectors, with coupling strength $\gamma \geqslant 0$, see Fig. 1(a). Specifically, the detectors monitor the state's local densities $\langle n_i \rangle \equiv \langle\psi|a_i^\dagger a_i|\psi\rangle$. The evolution of the system using a quantum trajectory description follows the stochastic Schrödinger equation (SSE) [4,37,51]

$$\begin{aligned} \mathrm{d}|\psi\rangle = &-iH\mathrm{d}t|\psi\rangle \\ &+\sum_{i=1}^{L}\left(\sqrt{\gamma}[n_i - \langle n_i\rangle]\mathrm{d}W_t^i - \frac{\gamma}{2}[n_i - \langle n_i\rangle]^2\mathrm{d}t\right)|\psi\rangle, \end{aligned} \tag{2}$$

where $\gamma$ is the coupling rate to the detectors (the measurement strength), and $\mathrm{d}W_t^i$ are Wiener increments with $\langle \mathrm{d}W_t^i \mathrm{d}W_{t'}^j\rangle = \delta_{i,j}\delta_{t,t'}\mathrm{d}t$. The particle's time evolution follows a stochastic sample path in space, a.k.a. quantum trajectory, see Fig. 1(c). Whenever a measurement occurs, the ballistic evolution of the trajectory is interrupted by a collapse (quantum jump). The

trajectory describes one possible sequence of measurement events and outcomes.

To account for all possible measurement sequences, one commonly samples the SSE for a large number $M \gg 1$ of quantum trajectories with equal initial conditions, i.e., $|\psi_i(t=0)\rangle = |L/2\rangle$, $i = 1, \ldots, M$. The average probability distribution of possible outcomes leads to a mixed state that is described by the density matrix $\rho = \overline{|\psi_i\rangle\langle\psi_i|} = \frac{1}{M}\sum_{i=1}^{M} |\psi_i\rangle\langle\psi_i|$. Alternatively, instead of an average over quantum trajectories, the evolution of the density matrix $\rho$ itself can be described by the Lindblad equation [4,37]

$$\partial_t \rho = -i[H, \rho] + \gamma \sum_{i=1}^{L} \left( n_i \rho n_i - \frac{1}{2}\{n_i, \rho\} \right). \tag{3}$$

For a finite measurement strength $\gamma > 0$, the dynamics of the density matrix of the initially localized particle changes from ballistic at times $t \lesssim 1/\gamma$ to diffusive at $t \gtrsim 1/\gamma$ [66], see Fig. 1(d). This transition is akin to a quantum-to-classical crossover. Interestingly, this crossover is not visible on the single trajectory level. In the following, we will characterize the crossover by comparing the entanglement in the system in both the quantum trajectory and the density matrix descriptions. Because entanglement is a nonlinear quantity (order parameter), we expect different results for the mixed state and the trajectory-averaged entanglement [32,37]. This has favored the use of trajectories rather than the Lindblad evolution to characterize measurement-induced entanglement dynamics [32,37,38].

For a 1D chain, entanglement describes the quantum correlations with respect to a cut at a bond $b$. To quantify entanglement, we employ the configuration coherence [47,48]

$$C_N(\rho, b) = 2 \sum_{\substack{i=1,\ldots,b \\ j=b+1,\ldots,L}} |\langle i|\rho|j\rangle|^2, \tag{4}$$

where $|j\rangle = a_j^\dagger|0\rangle$. For pure states, the configuration coherence is $C_N(|\psi\rangle, b) := C_N(|\psi\rangle\langle\psi|, b)$. The configuration coherence is a convex entanglement measure for mixed states under certain conditions, e.g., with a fixed number of particles subject to Lindblad evolution with Hermitian jump operators. For our case study, both the SSE (2) as well as the Linbdlad equation (3) fall under this category. For a single particle, the configuration coherence is related to the negativity $\mathcal{N}(\rho)$ [68]. In fact, $\sqrt{C_N(\rho)/2} = \mathcal{N}(\rho) \equiv (||\rho^{T_B}||_1 - 1)/2$, where $\rho^{T_B}$ is the partial transpose and $||\cdot||_1$ denotes the trace norm. In Figs. 1(e)–1(g), we plot the configuration coherence at each bond for the single particle evolutions discussed so far, cf. Figs. 1(b)–1(d). Without measurements ($\gamma = 0$), the particle ballistically evolves into a superposition over all sites, leading to the expansion of orbital entanglement across the chain, see Fig. 1(e). For finite $\gamma$, the quantum trajectory exhibits entanglement expansion with intermittent collapses, see Fig. 1(f). Crucially, we observe finite entanglement at long times $t \gg 1/\gamma$ for $\gamma > 0$. Conversely, the mixed state's entanglement vanishes around $t \approx 1/\gamma$, justifying the quantum-to-classical crossover labeling, see Fig. 1(g). As expected from Lindblad evolution, the density matrix $\rho$ evolves into a nonentangled infinite temperature state, $\rho(t \to \infty) = \mathbb{1}/L$. The time $t \approx 1/\gamma$ can be understood as the system's dephasing or Thouless' time

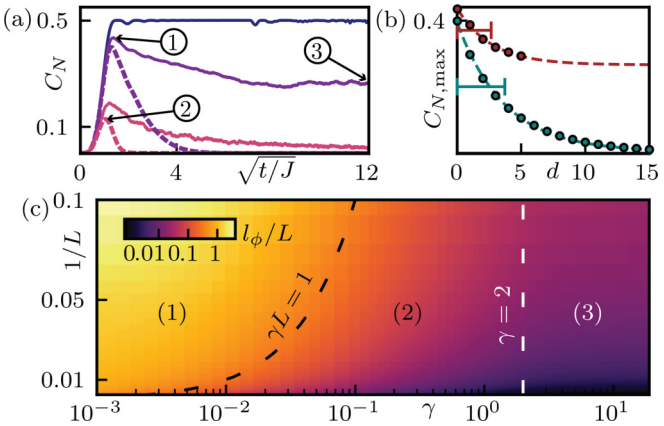


FIG. 2. (a) The configuration coherence at the middle bond as a function of time for quantum trajectories (solid lines) and the mixed state (dashed lines). Chain length is $L = 50$, trajectory values are averaged over $10^3$ runs, and measurement strengths are $\gamma = 0$, 0.1, 1 (blue, purple, pink). For $\gamma = 0$, the descriptions are equivalent. For finite $\gamma$, both descriptions show a maximum at an intermediate time [markers ①, ②] followed by a decay to a finite [marker ③] (zero) saturation value at long times for the trajectory (mixed state) description. (b) The maximal configuration coherence $C_{N,\max}$ as a function of the distance $d$ from the injection point of the single particle for measurement strength $\gamma = 0.1$ [cf. Eq. (5)]. An exponential fit (dashed lines) determines the coherence length $l_\phi$ for the mixed state (green) and $\lambda_\phi$ for trajectories (brown) marked by horizontal bars. (c) Phase diagram of the normalized single particle coherence length $l_\phi/L$ of the mixed state. We find three phases: (1) for small measurement strengths $\gamma \lesssim 1/L$, the particle coherently explores the full chain; (2) for intermediate measurement strengths $1/L \lesssim \gamma \lesssim 2$, the coherence length is finite and depends on the measurement strength, $l_\phi = l_\phi(\gamma)$; (3) for large measurement strengths $\gamma \gtrsim 2$, the coherence length saturates to $l_{\phi,\infty} \approx 0.3$.

[69,70]. Note that the vanishing entanglement at long times is the second motivation to favor quantum trajectories when studying measurement-induced phase transitions [30,37,38].

Now, we consider the time evolution of the configuration coherence and arrive at a definition for a $\gamma$-dependent coherence length. The coherence (Thouless) length describes the length scale over which the particle can evolve ballistically before the quantum-to-classical crossover turns its motion diffusive. This is reminiscent to defining an entanglement-based order parameter for describing the physics of our system, cf. Refs. [71–73]. Again, we inject the single particle at the center of the chain. First, we consider the average configuration coherence $\overline{C_N(|\psi_i\rangle, b)}$ over the quantum trajectories at any bond, $b = 1, \ldots, L-1$ [see Fig. 2(a)]: after it assumes a maximal value $\overline{C_N(|\psi_i\rangle, b)}_{\max}$ at intermediate times, it saturates to a $\gamma$-dependent finite value, $\overline{C_N(|\psi_i\rangle, b)}_\infty$, for $t \to \infty$. For each bond $b$ that satisfies $\overline{C_N(|\psi_i\rangle, b)}_{\max} > \overline{C_N(|\psi_i\rangle, b)}_\infty$, we plot the maximal configuration coherence as a function of the distance $d = |b - L/2|$ from the injection point, see Fig. 2(b). We find an exponential decay dependence:

$$\overline{C_N(|\psi_i\rangle, b)}_{\max} \propto \exp(-d/\lambda_\phi). \tag{5}$$

We use this decay to define the particle's coherence length $\lambda_\phi = \lambda_\phi(\gamma)$. Second, we consider the configuration coherence

evolution of the mixed state. The mixed state exhibits a maximal value at a similar intermediate time before it decays and vanishes, see Fig. 2(a). Again, we can extract the coherence length $l_\phi$ of the single particle as the length scale of the configuration coherence's exponential decay as a function of the distance from the injection point, $C_N(\rho, b)_{\max} \propto \exp(-d/l_\phi)$, see Fig. 2(b). Next, we analyze in more detail how the mixed state's coherence length depends on the measurement strength $\gamma$.

We use the mixed state entanglement analysis approach. The coherence length $l_\phi$ shows three distinct regimes as a function of the measurement strength $\gamma$, see Fig. 2(c): (1) For weak measurements $\gamma \lesssim 1/L$, the whole chain is explored coherently, and $l_\phi \gtrsim L$ is independent of the measurement strength. This is the regime of mesoscopic physics [70,74]. (2) For intermediate measurement strengths $2 \lesssim \gamma \lesssim 1/L$, the particle coherently explores a region of width $l_\phi \leqslant L$, beyond which it evolves diffusively. (3) For strong measurements $\gamma \gtrsim 2$, the coherence length saturates to $l_{\phi,\infty} \approx 0.3$. As such, scaling the system's size leads to three qualitatively different regions/phases. We employ the same analysis for the quantum trajectories and find a qualitatively similar behavior of the coherence length $\lambda_\phi$, see [61]: the crossover from (2) to (3) happens for $\gamma \approx 1.3$ and the saturating value is $\lambda_{\phi,\infty} \approx 1.7$. The observation of these regimes in the coherence length of the single-particle mixed state is the main result of our work.

The metallic-to-diffusive transition in the dynamics of our system has been studied in various setups [64–67]. The crossover from (1) to (3) can be understood as a sequence of underdamped-to-overdamped transitions of the Hamiltonian's plane wave eigenmodes (1). Specifically, each mode is damped by the measurement strength $\gamma$. With increasing $\gamma$, the modes become overdamped, starting with the slowest of the modes. At $\gamma \approx 2$, the fastest mode becomes overdamped, and the particle enters a regime where its coherent evolution is exponentially suppressed. As such, this transition does not depend on the choice of the initial state and can also be seen in the Liouvillian spectrum of the system, and obtained analytically in the two-sites case [61]. Note that such underdamped-to-overdamped transitions can also be observed in the spin-boson model [76] or in double quantum dots under dephasing [5]. It appears that such physics underpins the measurement-induced phase transition so that the latter lends an entanglement-based order parameter for the characterization of these effects [30,32,33,77]. As we find here, such characterization can be accomplished not only in quantum trajectories but also from the mixed state evolution.

The question remains of how our single-particle toy model (3) generalizes to many-body systems. For dilute systems, we postulate that the average interparticle distance $\delta$ will replace the system size $L$ as the relevant length scale, see Fig. 3(a). In the presence of strong measurements ($l_\phi < \delta/2$), the particles will not coherently experience each other. The many-body entanglement will then separate into a sum of single-particle contributions. The onset of many-body entanglement happens when the coherence length becomes of the order of half the inter-particle distance, $l_\phi \approx \delta/2$. In Fig. 3(b), we show such two-particle entanglement as a local maximum between the

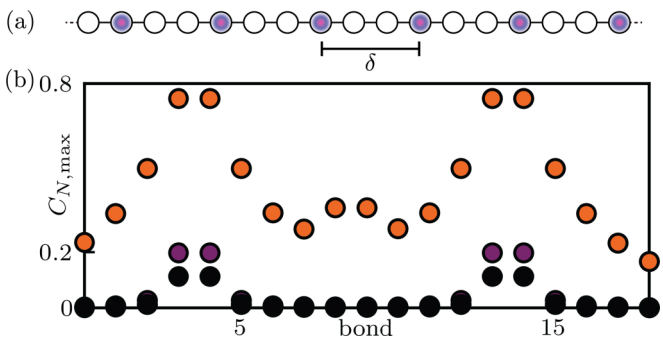


FIG. 3. (a) Chain with many particles homogeneously distributed with interparticle distance $\delta$. (b) Maximal configuration coherence for two particles on $L = 20$ sites, injected at sites 5 and 15, for measurement strengths $\gamma = 0.1,\ 1,\ 2$ (orange, purple, black). For $\gamma = 0.1$, two-particle entanglement between the two injection points builds up, because the particles coherently interact with each other. For large measurement strengths $\gamma = [1,\ 2]$, the maximal configuration coherence is the sum over the single-particle contributions. Our numerical implementation harnesses a matrix product density operator [75] representation of the mixed state.

two particles that cannot be described as a sum of single particle contributions [78–80]. For $l_\phi \ll \delta/2$, the entanglement will not depend on the chain length $L$ or the interparticle distance $\delta$. For $l_\phi \gtrsim \delta/2$, multiple particles can contribute to the configuration coherence and we, therefore, expect the entanglement to depend on the interparticle distance $\delta$. In light of the quantitative difference in the coherence lengths of the trajectories and the mixed state, we expect the onset of many-body entanglement at different values of the measurement strength $\gamma$.

We have analyzed the quantum measurement of a single particle using both quantum trajectories and a mixed-state Lindblad description. For both descriptions, we employed the recently developed configuration coherence as an entanglement measure [47,48]. At first sight, the entanglement behavior of the trajectories is opposite to that of the mixed state because the former remains finite at long times. At intermediate times, however, we extracted a coherence length from the entanglement and showed that it behaves qualitatively the same for both descriptions. Moreover, we found that the coherence length saturates at a finite value for large measurement strengths, namely when the fastest Liouvillian eigenmode becomes overdamped. Besides new insights into the quantum-to-classical crossover in terms of entanglement, our results provide evidence that the master equation can capture the measurement-induced entanglement dynamics of monitored systems. This observation unveils the underlying stochastic physics that measurements impart on the system, and their commonly observed manifestation in diffusive dynamics. In future work, we will extend the discussion to the many-body case.

We thank C. Leung for help with the quantum trajectory code, and M. H. Fischer and J. del Pino for fruitful discussions. The authors acknowledge financial support by ETH Research Grant ETH-51 201-1 and the Deutsche Forschungsgemeinschaft (DFG) - Project No. 449653034.

[1] E. Schrödinger, An undulatory theory of the mechanics of atoms and molecules, Phys. Rev. **28**, 1049 (1926).

[2] M. Born, Zur Quantenmechanik der Stoßvorgänge, Z. Phys. **37**, 863 (1926).

[3] J. von Neumann, *Mathematische Grundlagen der Quantenmechanik* (Springer Berlin, Heidelberg, 1996).

[4] H. M. Wiseman and G. J. Milburn, *Quantum Measurement and Control* (Cambridge University Press, Cambridge, 2009).

[5] S. A. Gurvitz, Measurements with a noninvasive detector and dephasing mechanism, Phys. Rev. B **56**, 15215 (1997).

[6] S. A. Gurvitz, Rate equations for quantum transport in multidot systems, Phys. Rev. B **57**, 6602 (1998).

[7] S. A. Gurvitz, L. Fedichkin, D. Mozyrsky, and G. P. Berman, Relaxation and the zeno effect in qubit measurements, Phys. Rev. Lett. **91**, 066801 (2003).

[8] H.-P. Breuer and F. Petruccione, *The Theory of Open Quantum Systems* (Oxford University Press, Oxford, 2002).

[9] G. Lindblad, On the generators of quantum dynamical semigroups, Commun. Math. Phys. **48**, 119 (1976).

[10] V. Gorini, A. Kossakowski, and E. C. G. Sudarshan, Completely positive dynamical semigroups of N-level systems, J. Math. Phys. **17**, 821 (1976).

[11] M. Thomas and A. Romito, Decoherence effects on weak value measurements in double quantum dots, Phys. Rev. B **86**, 235419 (2012).

[12] D. Manzano, A short introduction to the lindblad master equation, AIP Adv. **10**, 025106 (2020).

[13] S. Nakajima, On quantum theory of transport phenomena: Steady diffusion, Prog. Theor. Phys. **20**, 948 (1958).

[14] R. Zwanzig, Ensemble method in the theory of irreversibility, J. Chem. Phys. **33**, 1338 (1960).

[15] R. K. Wangsness and F. Bloch, The dynamical theory of nuclear induction, Phys. Rev. **89**, 728 (1953).

[16] F. Bloch, Generalized theory of relaxation, Phys. Rev. **105**, 1206 (1957).

[17] A. G. Redfield, The theory of relaxation processes, *Advances in Magnetic and Optical Resonance* (Elsevier, Amsterdam, 1965), Vol. 1, pp. 1–32.

[18] M. Tokuyama and H. Mori, Statistical-mechanical approach to random frequency modulations and the gaussian memory function, Prog. Theor. Phys. **54**, 918 (1975).

[19] M. Tokuyama and H. Mori, Statistical-mechanical theory of random frequency modulations and generalized Brownian motions, Prog. Theor. Phys. **55**, 411 (1976).

[20] H.-P. Breuer, B. Kappler, and F. Petruccione, The time-convolutionless projection operator technique in the quantum theory of dissipation and decoherence, Ann. Phys. **291**, 36 (2001).

[21] M. S. Ferguson, O. Zilberberg, and G. Blatter, Open quantum systems beyond fermi's golden rule: Diagrammatic expansion of the steady-state time-convolutionless master equations, Phys. Rev. Res. **3**, 023127 (2021).

[22] O. Zilberberg, A. Carmi, and A. Romito, Measuring cotunneling in its wake, Phys. Rev. B **90**, 205413 (2014).

[23] D. Bischoff, M. Eich, O. Zilberberg, C. Rössler, T. Ihn, and K. Ensslin, Measurement back-action in stacked graphene quantum dots, Nano Lett. **15**, 6003 (2015).

[24] M. S. Ferguson, L. C. Camenzind, C. Müller, D. E. F. Biesinger, C. P. Scheller, B. Braunecker, D. M. Zumbühl, and O. Zilberberg, Quantum measurement induces a many-body transition, arXiv:2010.04635 [cond-mat.mes-hall].

[25] O. Zilberberg, A. Romito, and Y. Gefen, Charge sensing amplification via weak values measurement, Phys. Rev. Lett. **106**, 080405 (2011).

[26] O. Zilberberg, A. Romito, D. J. Starling, G. A. Howland, C. J. Broadbent, J. C. Howell, and Y. Gefen, Null values and quantum state discrimination, Phys. Rev. Lett. **110**, 170405 (2013).

[27] O. Zilberberg, A. Romito, and Y. Gefen, Many-body manifestation of interaction-free measurement: The Elitzur-Vaidman bomb, Phys. Rev. B **93**, 115411 (2016).

[28] O. Zilberberg and A. Romito, Sensing electrons during an adiabatic coherent transport passage, Phys. Rev. B **99**, 165422 (2019).

[29] J. Johansson, P. Nation, and F. Nori, Qutip 2: A python framework for the dynamics of open quantum systems, Comput. Phys. Commun. **184**, 1234 (2013).

[30] Y. Li, X. Chen, and M. P. A. Fisher, Quantum zeno effect and the many-body entanglement transition, Phys. Rev. B **98**, 205136 (2018).

[31] M. Szyniszewski, A. Romito, and H. Schomerus, Entanglement transition from variable-strength weak measurements, Phys. Rev. B **100**, 064204 (2019).

[32] B. Skinner, J. Ruhman, and A. Nahum, Measurement-induced phase transitions in the dynamics of entanglement, Phys. Rev. X **9**, 031009 (2019).

[33] Y. Li, X. Chen, and M. P. A. Fisher, Measurement-driven entanglement transition in hybrid quantum circuits, Phys. Rev. B **100**, 134306 (2019).

[34] M. Szyniszewski, A. Romito, and H. Schomerus, Universality of entanglement transitions from stroboscopic to continuous measurements, Phys. Rev. Lett. **125**, 210602 (2020).

[35] C. Noel, P. Niroula, D. Zhu, A. Risinger, L. Egan, D. Biswas, M. Cetina, A. V. Gorshkov, M. J. Gullans, D. A. Huse, and C. Monroe, Measurement-induced quantum phases realized in a trapped-ion quantum computer, Nat. Phys. **18**, 760 (2022).

[36] J. M. Koh, S.-N. Sun, M. Motta, and A. J. Minnich, Experimental realization of a measurement-induced entanglement phase transition on a superconducting quantum processor, arXiv:2203.04338 [quant-ph].

[37] X. Cao, A. Tilloy, and A. D. Luca, Entanglement in a fermion chain under continuous monitoring, SciPost Phys. **7**, 024 (2019).

[38] Y. Bao, S. Choi, and E. Altman, Theory of the phase transition in random unitary circuits with measurements, Phys. Rev. B **101**, 104301 (2020).

[39] M. A. Nielsen and I. L. Chuang, *Quantum Computation and Quantum Information: 10th Anniversary Edition* (Cambridge University Press, Cambridge, 2010).

[40] L. Gurvits, Classical deterministic complexity of edmonds' problem and quantum entanglement, arXiv:quant-ph/0303055 [quant-ph].

[41] S. Gharibian, Strong NP-hardness of the quantum separability problem, arXiv:0810.4507 [quant-ph].

[42] J. Preskill, Quantum Computing in the NISQ era and beyond, Quantum **2**, 79 (2018).

[43] M. Brooks, Beyond quantum supremacy: the hunt for useful quantum computers, Nature (London) **574**, 19 (2019).

[44] V. Giovannetti, S. Lloyd, and L. Maccone, Advances in quantum metrology, Nat. Photon. **5**, 222 (2011).

[45] L. Pezzè, A. Smerzi, M. K. Oberthaler, R. Schmied, and P. Treutlein, Quantum metrology with nonclassical states of atomic ensembles, Rev. Mod. Phys. **90**, 035005 (2018).
[46] S. Pirandola, B. R. Bardhan, T. Gehring, C. Weedbrook, and S. Lloyd, Advances in photonic quantum sensing, Nat. Photon. **12**, 724 (2018).
[47] E. van Nieuwenburg and O. Zilberberg, Entanglement spectrum of mixed states, Phys. Rev. A **98**, 012327 (2018).
[48] C. Carisch and O. Zilberberg, Efficient separation of quantum from classical correlations for mixed states with a fixed charge, Quantum **7**, 954 (2023).
[49] O. Alberton, M. Buchhold, and S. Diehl, Entanglement transition in a monitored free-fermion chain: From extended criticality to area law, Phys. Rev. Lett. **126**, 170602 (2021).
[50] M. Buchhold, Y. Minoguchi, A. Altland, and S. Diehl, Effective theory for the measurement-induced phase transition of dirac fermions, Phys. Rev. X **11**, 041004 (2021).
[51] X. Turkeshi, A. Biella, R. Fazio, M. Dalmonte, and M. Schiró, Measurement-induced entanglement transitions in the quantum Ising chain: From infinite to zero clicks, Phys. Rev. B **103**, 224210 (2021).
[52] X. Turkeshi, M. Dalmonte, R. Fazio, and M. Schirò, Entanglement transitions from stochastic resetting of non-Hermitian quasiparticles, Phys. Rev. B **105**, L241114 (2022).
[53] M. Fava, L. Piroli, T. Swann, D. Bernard, and A. Nahum, Nonlinear sigma models for monitored dynamics of free fermions, arXiv:2302.12820 [cond-mat.stat-mech].
[54] Y. L. Gal, X. Turkeshi, and M. Schirò, Volume-to-area law entanglement transition in a non-Hermitian free fermionic chain, SciPost Phys. **14**, 138 (2023).
[55] G. Kells, D. Meidan, and A. Romito, Topological transitions in weakly monitored free fermions, SciPost Phys. **14**, 031 (2023).
[56] M. Szyniszewski, O. Lunt, and A. Pal, Disordered monitored free fermions, Phys. Rev. B **108**, 165126 (2023).
[57] P. Pöpperl, I. V. Gornyi, and Y. Gefen, Measurements on an Anderson chain, Phys. Rev. B **107**, 174203 (2023).
[58] M. Coppola, E. Tirrito, D. Karevski, and M. Collura, Growth of entanglement entropy under local projective measurements, Phys. Rev. B **105**, 094303 (2022).
[59] J. Merritt and L. Fidkowski, Entanglement transitions with free fermions, Phys. Rev. B **107**, 064303 (2023).
[60] I. Poboiko, P. Pöpperl, I. V. Gornyi, and A. D. Mirlin, Theory of free fermions under random projective measurements, arXiv:2304.03138 [quant-ph].
[61] See Supplemental Material at http://link.aps.org/supplemental/10.1103/PhysRevResearch.5.L042031 for a scaling analysis of the mixed state coherence length; details on the extraction of the saturating measurement strength; a phase diagram and discussion of the quantum trajectory coherence length; an analysis of the Liouvillian spectrum and the underdamped-to-overdamped transitions of its eigenmodes; an analytical discussion of the underdamped-to-overdamped transition for a single particle on two sites; a procedure to calculate the configuration coherence for fermionic Gaussian states. It also contains Refs. [5,37,81–84].
[62] J. Kempe, Quantum random walks: An introductory overview, Contemp. Phys. **44**, 307 (2003).
[63] K. Schönhammer, Unusual broadening of wave packets on lattices, Am. J. Phys. **87**, 186 (2019).
[64] M. Esposito and P. Gaspard, Emergence of diffusion in finite quantum systems, Phys. Rev. B **71**, 214302 (2005).
[65] D. Basko, I. Aleiner, and B. Altshuler, Metal–insulator transition in a weakly interacting many-electron system with localized single-particle states, Ann. Phys. **321**, 1126 (2006).
[66] A. Amir, Y. Lahini, and H. B. Perets, Classical diffusion of a quantum particle in a noisy environment, Phys. Rev. E **79**, 050105(R) (2009).
[67] M. Žnidarič, Dephasing-induced diffusive transport in the anisotropic Heisenberg model, New J. Phys. **12**, 043001 (2010).
[68] G. Vidal and R. F. Werner, Computable measure of entanglement, Phys. Rev. A **65**, 032314 (2002).
[69] J. T. Edwards and D. J. Thouless, Numerical studies of localization in disordered systems, J. Phys. C **5**, 807 (1972).
[70] E. Akkermans and G. Montambaux, *Mesoscopic Physics of Electrons and Photons* (Cambridge University Press, Cambridge, 2007).
[71] A. Bayat, H. Johannesson, S. Bose, and P. Sodano, An order parameter for impurity systems at quantum criticality, Nat. Commun. **5**, 3784 (2014).
[72] M. Iqbal and N. Schuch, Entanglement order parameters and critical behavior for topological phase transitions and beyond, Phys. Rev. X **11**, 041014 (2021).
[73] L. Stocker, S. H. Sack, M. S. Ferguson, and O. Zilberberg, Entanglement-based observables for quantum impurities, Phys. Rev. Res. **4**, 043177 (2022).
[74] Y. Imry, *Introduction to Mesoscopic Physics*, Mesoscopic physics and nanotechnology (Oxford University Press, Oxford, 2002).
[75] F. Verstraete, J. J. García-Ripoll, and J. I. Cirac, Matrix product density operators: Simulation of finite-temperature and dissipative systems, Phys. Rev. Lett. **93**, 207204 (2004).
[76] A. J. Leggett, S. Chakravarty, A. T. Dorsey, M. P. A. Fisher, A. Garg, and W. Zwerger, Dynamics of the dissipative two-state system, Rev. Mod. Phys. **59**, 1 (1987).
[77] A. Biella and M. Schiró, Many-body quantum Zeno effect and measurement-induced subradiance transition, Quantum **5**, 528 (2021).
[78] A. Lukin, M. Rispoli, R. Schittko, M. E. Tai, A. M. Kaufman, S. Choi, V. Khemani, J. Léonard, and M. Greiner, Probing entanglement in a many-body–localized system, Science **364**, 256 (2019).
[79] H. B. Kaplan, L. Guo, W. L. Tan, A. De, F. Marquardt, G. Pagano, and C. Monroe, Many-body dephasing in a trapped-ion quantum simulator, Phys. Rev. Lett. **125**, 120605 (2020).
[80] L.-N. Wu and A. Eckardt, Prethermal memory loss in interacting quantum systems coupled to thermal baths, Phys. Rev. B **101**, 220302(R) (2020).
[81] V. M. Kenkre and D. W. Brown, Exact solution of the stochastic liouville equation and application to an evaluation of the neutron scattering function, Phys. Rev. B **31**, 2479 (1985).
[82] M. V. Medvedyeva, F. H. L. Essler, and T. Prosen, Exact bethe ansatz spectrum of a tight-binding chain with dephasing noise, Phys. Rev. Lett. **117**, 137202 (2016).
[83] M. Žnidarič, Relaxation times of dissipative many-body quantum systems, Phys. Rev. E **92**, 042143 (2015).
[84] Z. Cai and T. Barthel, Algebraic versus exponential decoherence in dissipative many-particle systems, Phys. Rev. Lett. **111**, 150403 (2013).